

Mechanics of a Porous Web Moving Over a Cylindrical Guide

Sinan Müftü

Haystack Observatory,
Massachusetts Institute of Technology,
Westford, MA 01886

M. Cengiz Altan

School of Aerospace and Mechanical
Engineering,
The University of Oklahoma,
Norman, OK 73019

A model for analyzing the interfacial conditions of a porous web moving over a cylindrical rigid guide is presented. This problem is different from the classical foil bearing problem due to the fact that the air can diffuse through the porous web itself. A micro-mechanics model is used to express the web porosity as a function of the fiber volume fraction of the web. Darcy's law is used to account for the air flow and pressure drop across the web thickness, and a new modified Reynolds equation is derived to model the airflow in the web-guide interface. The porous web is modeled as a moving cylindrically curved beam, and the solid-body contact between the web and the guide is modeled using an asperity compliance function. The governing equations are nondimensionalized and important nondimensional parameters are identified. The coupled nonlinear steady-state system is solved using a modified Newton-Raphson algorithm. The traction characteristics of the web are presented for different porosity levels, asperity height, and compliance. [S0742-4787(99)00102-8]

Introduction

In this paper, a model for analyzing the traction behavior of a permeable web moving over a cylindrical guide is presented. Paper, textiles, and filters are examples of permeable materials handled in thin, deformable, and continuous sheets called webs. Most paper, textile, and filter webs have complex microstructures formed by continuous or discontinuous slender fibers. Air can diffuse through these fibrous web structures if a pressure gradient is applied across their thickness. Such pressure gradients occur due to air entrainment when a web moves over rotating or stationary guides in web handling machinery as shown in Fig. 1. For example in paper handling machines webs travel at speeds reaching 25 m/s. This creates a potential for self-air lubrication between the web and the rigid guide. Based on experimental studies, Daly [1] and Ducotey and Good [2] indicate that air entrainment can cause traction loss for paper webs that have low permeability at some combinations of the web handling parameters such as speed, web tension, and guide radius.

This problem is similar to the classical foil bearing problem where air entrained in the entry region of the web-guide interface can flow out at the lateral edges and at the exit region of the interface [3]. In the case of a porous web, air also flows out through the interstices inside the web (see Fig. 2). Therefore the equations governing the air flow in the interface should be modified to take into account the effect of airflow through the porous web.

Hashimoto [4,5] studied the transport of an impermeable web over an externally pressurized porous guide where the effect of incoming air is included by modifying the Reynolds equation with a source term. Müftü and Benson [6] presented a modified version of the Reynolds equation which incorporates air diffusion through a moving web using Darcy's law, where air in the web-guide clearance is assumed to be compressible. This work focused on the steady motion of a web wrapped over a stationary air bar. Wang [7] considered the transient motion of a flat web traveling between two stationary air bars that are used as flutter suppression devices. Permeability was incorporated into the incompressible version of the Reynolds equation. Ducotey and Good presented experimental studies of factors affecting the traction loss of impermeable [8] and permeable [2] webs over rollers.

When a web under tension T moves over a stationary cylindrical

guide with radius R , its tension increases by an amount ΔN in the moving direction of the web, due to sliding friction. In the absence of self-air lubrication, the contact pressure in the web-guide interface equals the belt-wrap pressure T/R and the tension increase can be predicted by the well-known belt-wrap formula,

$$\frac{\Delta N}{T} = (e^{f\beta} - 1) \quad (1)$$

where f is the kinetic coefficient of friction and β is the wrap angle [9]. However, the self-air lubrication in the interface could cause air pressure to rise to such levels that the web is *partially* or *fully* supported over an air layer. In the case when the web is fully supported by air, traction over the guide will be lost and no tension increase will occur over the guide. On the other hand, when the web is only partially supported by air pressure, contact will occur in some part of the web-guide interface. In this case the contact pressure will no longer be equal to the belt-wrap pressure. The tension change cannot be predicted by the belt-wrap formula, unless an *equivalent friction coefficient* is measured. The experimental work of Ducotey and Good [8] adopts this approach.

In this paper, the coefficient of friction f is treated as a constant, independent of the web speed. The tension change is found from the in-plane force equilibrium of the web. As a result of sliding, a shear stress τ develops on the contacting surface of the web. Based on Amonton's law of sliding friction [9], it is assumed that this shear stress is proportional to the contact pressure p_c as follows:

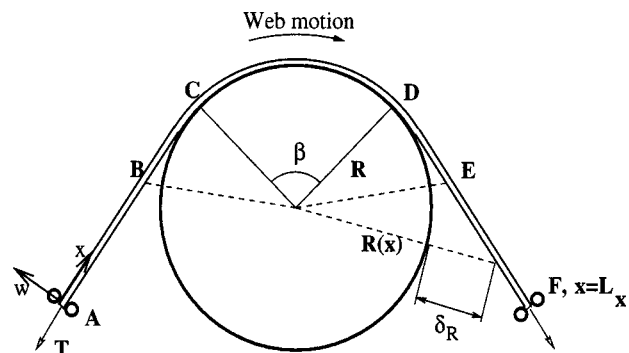


Fig. 1 Schematic view of a web transported over a guide with speed V_x and under tension T

Contributed by the Tribology Division for publication in the JOURNAL OF TRIBOLOGY. Manuscript received by the Tribology Division March 17, 1999; revised manuscript received July 6, 1999. Associate Technical Editor: J. Frene.

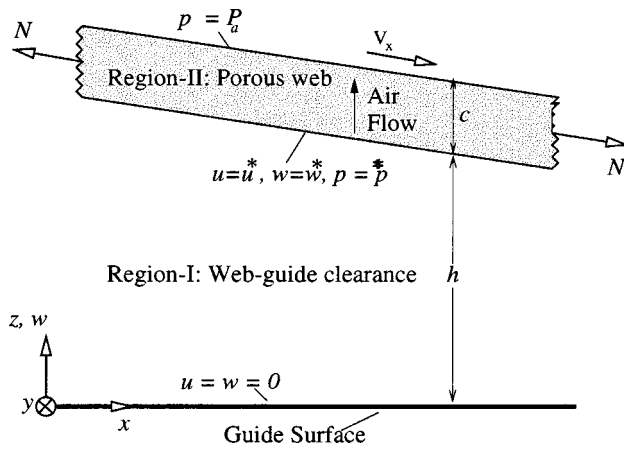


Fig. 2 Schematic view of a porous web moving over a stationary guide

$$\tau = \begin{cases} -fp_c, & \text{for } V_x > 0, \\ fp_c, & \text{for } V_x < 0, \end{cases} \quad (2)$$

where the web speed V_x is positive for a web moving in the increasing x direction as shown in Fig. 1. The shear stress that would occur due to the interaction of air and the web is neglected. In this work, the change in web tension due to sliding friction is calculated by obtaining a simultaneous solution of the in-plane and out-of-plane web equilibrium with contact and self-air lubrication through a permeable web.

The analysis performed in this paper considers two lubrication regimes depending on where and if the web contacts the guide. Full *hydrodynamic lubrication* takes place in the interface if the web is fully supported by air, or under the noncontact region if the web is supported by air, only in one part of the wrap region. *Mixed lubrication* takes place in the contact region where the web-guide spacing is limited by the heights of the surface asperities. The exact value of the web-guide spacing depends on the local equilibrium conditions, due to the compliant nature of the asperities: Under normal operating conditions this clearance is not expected to close completely. It is assumed that while the surfaces contact on the peak of the asperities, air can move along the interface in the valleys. In this case, the Couette-flow contributes to air lubrication in the contact region. In calculating the air pressure, the effects of surface roughness on the airflow as described, for example, by Patir and Chang [10] are not considered. In this analysis the air pressure for both lubrication regimes is obtained by solving the modified Reynolds equation.

A Micromechanics Model for the Web Permeability

In order to describe the airflow through a porous web, the permeability of the web needs to be characterized. It is possible to perform a parametric study of web dynamics within an approximate permeability range without being concerned about the effect of web microstructure. However, it is beneficial to develop flow models to predict web permeability only based on the web microstructure. Then an a priori estimate of the permeability becomes possible from the microscopic analysis of the web.

The fibrous porous media are inherently anisotropic, thus the permeability is characterized by a second order tensor. Microstructural considerations of the porous media are empirically included in the classical Kozeny-Carmen equation. In this widely used model, one can estimate the permeability using superficial microstructure descriptors such as tortuosity, shape factor, hydraulic radius, and specific wetted-surface. For anisotropic media the use of modified Kozeny-Carmen equation has been proposed, introducing an anisotropic Kozeny-Carmen constant [11–13]. In this approach, the shape factor or hydraulic radius is redefined

from a phenomenological viewpoint. Since the geometrical details of the anisotropic media (i.e., arrangement of the fibers) is not considered in these models, the permeability predictions may deviate considerably from the results obtained by numerical simulations [14]. For isotropic porous media such as granular materials, a single permeability κ is defined. For such cases, the microstructure can be fully defined by simpler models using representative pore diameter and porosity [15].

In this paper, a permeability model based on the microstructural arrangement of the fibers [14] is implemented. As the fibers within the web are primarily planar, effects of through-the-thickness fiber orientation on the permeability are not considered. It is also assumed that the fibers have uniform radius with cylindrical cross sections, and either have large aspect ratios (i.e., paper) or are continuous (i.e., some filters, textiles), thus neglecting end effects. Consequently, the local microscopic flow can be assumed to take place across fiber bundles through the web thickness. Since the fiber diameter is usually much smaller than the web thickness, a number of fiber layers with some repetitive pattern exist through the web thickness. The actual description of fiber arrangement through the web thickness is rather difficult as fibers are more likely to form patterns without any long range order. Yet a hexagonal fiber arrangement may be used to represent the porous microstructure, as it enables to model lowest possible porosity formed by cylindrical fibers (i.e., $1 - \pi/2\sqrt{3} \approx 9.3\%$). If one considers that the porosity of most of the paper or textile webs are rather low (i.e., 10–30%), the use of hexagonal packing order is particularly useful in such practical applications. Based on these geometric considerations, the Stoke's flow across the fiber arrays can be assumed at the micro-scale. In addition, the flow is modeled to take place through the interstitial channels of variable thickness formed by the cylindrical fibers. The pressure drop in the flow direction is only due to viscous forces and can be obtained analytically by integrating the pressure gradient over the length of a repeating unit cell. This relation can be used to obtain a closed-form permeability expression as a function of the web porosity. In fibrous porous media, it is customary to use fiber volume fraction ($\phi = 1 - \text{porosity}$) instead of porosity. Following this convention, the nondimensional transverse permeability of a fibrous web can be expressed in terms of its fiber volume fraction as [14]

$$\frac{\kappa}{r^2} = \frac{1}{3\sqrt{3}} \frac{(1-l^2)^2}{l^3} \left(3l \frac{\tan^{-1}\left(\sqrt{\frac{1+l}{1-l}}\right)}{\sqrt{1-l^2}} + \frac{1}{2}l^2 + 1 \right)^{-1}, \quad (3)$$

$$l^2 = \frac{2\sqrt{3}}{\pi} \phi,$$

where r is the fiber radius.

An Air Lubrication Model with a Permeable Web

In the presence of a porous web, the air that is entrained between the web and the rigid guide will flow out partly through the pores and partly from the lateral edges of the web. The airflow in the web-guide interface is considered in two regions as depicted in Fig. 2. In Region-I, $0 \leq z \leq h$, the air is between the surface of the guide and the porous web. This flow region is referred to as the web-guide clearance. The distance between the web and the guide is indicated by h . In Region-II, $h \leq z \leq h + c$, the air is inside the porous web, where c is the web thickness.

For a typical web-guide interface with self-air lubrication, the flow is characterized by a modified Reynolds number $\text{Re}^* = \rho V h_o^2 / \mu L_b$ [3]. This Reynolds number is at the order of $10^{-4} - 10^{-5}$ for typical web handling processes. For example, using air density $\rho = 1.2 \text{ kg/m}^3$, air viscosity $\mu = 1.82 \times 10^{-5} \text{ Pa}\cdot\text{s}$, bearing length $L_b = 0.25 \text{ m}$, web speed $V = 10 \text{ m/s}$, and web-guide clearance $h_o = 5 \mu\text{m}$, the modified Reynolds number Re^* is 6.6

$\times 10^{-5}$. As the modified Reynolds number is significantly smaller than one, the effect of fluid inertia is negligible. In the temperature range that is of practical interest, it can be assumed that the air viscosity is constant and the flow is isothermal. Therefore, the air pressure and the density are related by $p = C\rho$, where C is a constant that includes the universal gas constant and the ambient air temperature. In a web handling application, the thickness of the air film is much smaller than the other dimensions of the problem. Therefore, it can be assumed that the air pressure is constant through the thickness of the air layer in Region-I. The analysis shown below will assume that the web is infinitely wide. Therefore, only the longitudinal and transverse components of the air velocity, namely u and w , will be considered. Extension to finite width case is straightforward and can be found in Müftü and Benson [6].

In the web-guide clearance, the fluid flow is governed by the viscous stress gradients through the lubrication zone. Thus the Navier-Stokes equations simplify as

$$\text{In Region-I: } \frac{\partial p}{\partial x} = \mu \frac{\partial^2 u}{\partial z^2}, \quad (4)$$

where p is the air pressure. At steady state, the airflow inside a moving porous medium, such as a web, is governed by Darcy's law [16],

$$\text{In Region-II: } u^* = V_x - \frac{\kappa}{\mu} \frac{\partial p^*}{\partial x}, \quad (5a)$$

$$w^* = -\frac{\kappa}{\mu} \frac{\partial p^*}{\partial z}, \quad (5b)$$

where V_x is the web speed and * over the variables indicates that they are defined for Region-II. In Eq. (5a) the airflow in the plane of the porous web is adjusted for the motion of the web. The micromechanical component of the airflow is proportional to the pressure gradient and permeability κ , and inversely proportional to air viscosity μ . The conservation of mass in Regions-I and -II is governed by

$$\text{In Region-I: } \frac{\partial \rho u}{\partial x} + \frac{\partial \rho w}{\partial z} = 0, \quad (6a)$$

$$\text{In Region-II: } \frac{\partial \rho^* u^*}{\partial x} + \frac{\partial \rho^* w^*}{\partial z} = 0. \quad (6b)$$

The edges of the lubrication zone are located at $x = x_B$ and x_E , sufficiently¹ far away from the tangency points, $x = x_C$ and x_D , as shown in Fig. 1. The boundary conditions for the fluid flow at the outside boundaries of the combined Regions-I and -II are

$$\text{At } x = x_B, x_E: \quad p = P_a, \quad (7a)$$

$$\text{At } z = 0: \quad u = 0, \quad (7b)$$

$$\text{At } z = 0: \quad w = 0, \quad (7c)$$

$$\text{At } z = h + c: \quad p = P_a, \quad (7d)$$

where P_a is the ambient air pressure. At the interface of the Regions-I and -II (i.e., $z = h$), the following matching conditions are needed:

$$u = u^*, \quad (8a)$$

$$w = w^*, \quad (8b)$$

$$p = p^*. \quad (8c)$$

¹In the regular foil bearing problem, the length of the entry and exit regions, L_e , are on the order of $h_o / (6\mu V/T)^{1/3}$ (Gross [3], p. 490). Using the typical web handling parameters given above, with web tension $T = 75$ N/m, an L_e value of 0.2 mm is found. The lengths |BC| and |DE| shown in Fig. 1 are chosen several orders of magnitude larger than L_e .

Equations (4)–(8) represent the airflow in the porous web interface. Rather than attempting a simultaneous solution of these equations, a simplified equation, similar to the well-known Reynolds equation is derived. This is achieved by assuming that the fluid is incompressible inside the web, and that the fluid velocity, w^* , varies linearly in the z direction. Assumptions similar to the second one have been made by Bujurke et al. [17] and Tichy [16], and indicate that the length scales in the running direction are much larger than in the thickness direction. The incompressibility assumption is introduced in order to be able to integrate the equation in the z direction, and should be acceptable as a first order approximation.

The details of this derivation are given by Müftü and Benson [6]. This derivation involves integrating the mass conservation equation for Regions-I and -II in the z -direction, substituting Eqs. (4) and (5) and the appropriate matching and boundary conditions. The modified Reynolds equation for a moving porous medium then becomes

$$\frac{\partial}{\partial x} \left(ph^3 \frac{\partial p}{\partial x} \right) - \frac{12\kappa}{c} p(p - P_a) + 6\kappa \left[cp \frac{\partial^2 p}{\partial x^2} + \frac{\partial}{\partial x} \left(ph \frac{\partial p}{\partial x} \right) - 2p \frac{\partial h}{\partial x} \frac{\partial p}{\partial x} \right] = 12\mu V_x \left(\frac{1}{2} \frac{\partial(p h)}{\partial x} - p \frac{\partial h}{\partial x} \right). \quad (9)$$

Note that for an impermeable web (i.e., $\kappa = 0$), the classical Reynolds equation for compressible flow is recovered.

The Web Displacement Equations

A model for the moderately large web deformations, using a self-adjusting reference state, has been recently presented by Müftü and Cole [18]. Their model allows keeping a constant web tension when the web length changes as a result of external pressurization under the web. Here a similar model is introduced where web strains are measured from the quiescent contact equilibrium state of the web, rather than from an ideally smooth reference surface.

When an initially flat web is wrapped around a guide with radius R , under tension N , as shown in Fig. 1, its radius of curvature along a coordinate axis placed on the web is given by [18]

$$\frac{1}{R(x)} = \frac{1}{R} \begin{cases} e^{-(1+(x_C-x)/b)}, & 0 \leq x \leq x_C \\ 1, & x_C \leq x \leq x_D \\ e^{-(1+(x-x_D)/b)}, & x_D \leq x \leq L_x \end{cases} \quad (10)$$

where $b = (D/N)^{1/2}$ is the characteristic bending length and $D = Ec^3/12(1-\nu^2)$ is the bending stiffness, calculated by using the elastic modulus E , Poisson's ratio ν , and thickness c of the web. The wrap region spans between the tangency points x_C , x_D , and its length is $L = R\beta$. The web curvature causes (i) the curved part of the web gain an additional in-plane shell stiffness, $k = Ec/R(x)^2(1-\nu^2)$ and (ii) a belt-wrap pressure, $N/R(x)$, acting in the radially inward direction.

External forces acting on the web originate from three sources. These are the contact pressure p_c , the air pressure p , and the tangential shear stress τ , which are due to rigid body contact, self-air lubrication, and sliding, respectively. The contact and air pressures act in the opposite direction to the belt-wrap pressure. These forces are balanced by the bending resistance and in-plane stiffness of the web. The normal displacement w' of a web moving with a speed V_x is obtained by solving the following differential equation:

$$D \frac{d^4 w'}{dx^4} + k w' - (N - \rho_a V_x^2) \frac{d^2 w'}{dx^2} - \frac{dN}{dx} \frac{dw'}{dx} = (p - P_a) + p_c - \frac{N}{R(x)}, \quad (11)$$

where ρ_a is the mass of the web per unit area [18]. The mass of the web per unit area ρ_a can be calculated from the density of the web material, ρ_{mat} , the web thickness, c , fiber volume fraction of the web, ϕ , and density of air, ρ , by using $\rho_a = [\rho_{mat}\phi + \rho(1 - \phi)]c$. The inertial loads reduce the web tension by an amount $\rho_a V_x^2$ as shown in Eq. (11).

As it will be shown later in Eq. (16), the contact pressure p_c acts on the web, only when the web-guide spacing falls below a specific asperity engagement height, σ_o . In this case, mixed lubrication takes place in the interface and the web is supported by the combined contact and air pressures as shown on the right-hand side of Eq. (11). The corresponding air pressure p is calculated from the modified Reynolds equation. When the web-reverser clearance h is higher than σ_o , hydrodynamic lubrication takes place. In this case, the web is supported by air pressure and contact pressure becomes zero. The corresponding air pressure is again calculated from the solution of the modified Reynolds equation.

When self-air lubrication in the interface causes the contact pressure distribution to differ from N/R , the tension change due to sliding friction should be calculated from the in-plane stress equilibrium of the web. This equation, for an infinitely wide web, is given as follows [18]:

$$\frac{dN}{dx} = -\tau, \quad (12)$$

where τ is the external shear stress acting on the contacting surface of the web, given by Eq. (2). Equation (12) assumes that the only external shear stress acting on the web is due to friction caused by sliding in the contact region.

The equilibrium Eqs. (11) and (12) are subject to the following boundary conditions:

$$\text{At } x=0: \quad w' = 0, \quad \frac{d^2 w'}{dx^2} = 0, \quad (13a)$$

$$\text{At } x=L_x: \quad w' = 0, \quad \frac{d^2 w'}{dx^2} = 0, \quad (13b)$$

$$\text{At } x=0: \quad N = T. \quad (13c)$$

Equations (13a,b) indicate that the web is simply supported, and Eq. (13c) indicates that the web tension is fixed on the left boundary.

As a result of choosing a coordinate axis oriented along the web, we have $w' = h$ in the wrap-region, where h is the web-guide clearance. Outside the wrap-region the clearance is measured perpendicular to the surface of the guide [19]. In general, the clearance is calculated as

$$h = w' + \delta, \quad (14)$$

where δ is a function representing the shape of the cylindrical guide in the x coordinate along the web. This function is given as

$$\delta(x) = \delta_L(x)[1 - H(x - x_C)] + \delta_R(x)H(x - x_D), \quad (15)$$

where H is the Heaviside step function, and δ_L and δ_R represent the normal distance between the guide surface and the undeformed web, as shown in Fig. 1.

In practice, contact between two surfaces occurs on the asperities of the surfaces [20]. A simple model for the deformation of these asperities, in response to increasing apparent contact pressure, is a set of nonlinear springs that are attached on each surface, as shown in Fig. 3. This empirically based model has been used for the head-tape interface problem [21],

$$p_c = p_o(1 - h/\sigma_o)^2 \mathcal{H}, \quad (16)$$

$$\mathcal{H} = [1 - H(h - \sigma_o)],$$

where p_o is the asperity compliance parameter and σ_o is the asperity engagement height obtained experimentally. The function

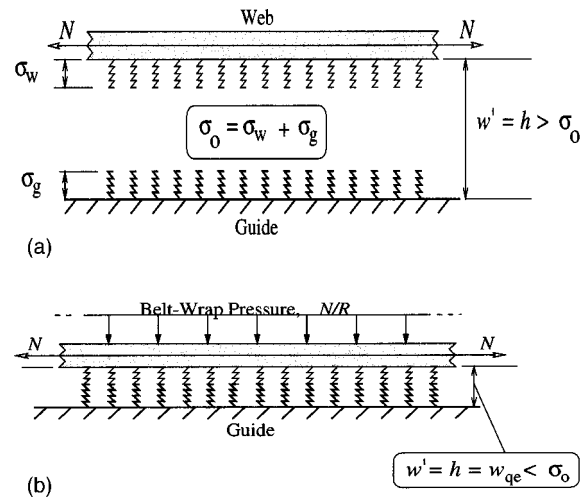


Fig. 3 Schematic view of the reference state of the web showing the contact and no-contact regions. (a) Web-guide spacing in no-contact region. (b) Quiescent web in contact region.

\mathcal{H} insures that contact pressure is not applied if $h > \sigma_o$. Non-empirical contact pressure functions such as the one developed by Greenwood and Williamson [22] exist but are not considered in this work.

The contact pressure parameters p_o and σ_o are usually obtained by experiments where the web-guide spacing is carefully measured as a function of apparent contact pressure [21]. These parameters represent the combined measured characteristics of the two contacting surfaces. A recent study by Rice et al. [23] shows that the combined asperity engagement height σ_o , for a wide range of webs, can be calculated based on a specific combination of the easily measurable surface topography parameters of average peak-to-valley and average peak height. This study also showed that the magnitude of the asperity compliance parameter has a small influence on the final equilibrium results.

Reference State Adjustment for Web Deformations in Contact Problems. When a quiescent web is pulled over a cylindrical guide, asperities of the two surfaces are compressed until the belt-wrap pressure N/R is balanced by the contact pressure p_c . At this state, which can be called the quiescent equilibrium state, the web displacement is indicated by $w' = w_{qe}$ as shown in Fig. 3(b). Note that except for the edges, w_{qe} is uniform in the wrap-region.

This definition of the contact equilibrium presents a problem which can be shown by substituting w_{qe} into Eq. (11),

$$kw_{qe} = p_c - \frac{N}{R}. \quad (17)$$

The left-hand side term kw_{qe} is due to the resistance of the web to circumferential expansion. However, the expansion caused by setting the web to its equilibrium state on top of the asperities should not cause strains in the web, but rather should cause a slightly longer web span between the supports. Therefore, the proper reference for web strains in the quiescent equilibrium state, and not the ideally smooth surfaces. This is implemented by using

$$w = w' - w_{qe} \quad (18)$$

in Eq. (11). For small values of σ_o , such as 50–100 nm for magnetic tapes, the difference is negligibly small. However, for rougher surfaces such as paper, with a typical $\sigma_o \approx 5 \mu\text{m}$ or higher, a significant error would be introduced into equilibrium if the reference state adjustment is not considered.

Normalization of the Governing Equations

The equations for the airflow, web deformation, and tension variation (i.e., Eqs. (9), (11), and (12), respectively) need to be nondimensionalized to identify the relevant nondimensional parameter groups and investigate how these groups affect the web motion. In addition, nondimensionalization simplifies the governing equations by reducing the large number of independent variables.

The nondimensional equation for airflow can be expressed as

$$\begin{aligned} \frac{d}{d\bar{x}} \left(\bar{p} \bar{h}^3 \frac{d\bar{p}}{d\bar{x}} \right) - A \left\{ \bar{p}(\bar{p}-1) + \left(\frac{c}{L} \right)^2 \left[\bar{p} \frac{d^2 \bar{p}}{d\bar{x}^2} + \left(\frac{\sigma_o}{c} \right) \right. \right. \\ \left. \left. \times \left(\frac{d}{d\bar{x}} \left(\bar{p} \bar{h} \frac{d\bar{p}}{d\bar{x}} \right) - 2\bar{p} \frac{d\bar{h}}{d\bar{x}} \frac{d\bar{p}}{d\bar{x}} \right) \right] \right\} \\ = 2B \left(\frac{1}{2} \frac{d(\bar{p}\bar{h})}{d\bar{x}} - \bar{p} \frac{d\bar{h}}{d\bar{x}} \right) \end{aligned} \quad (19)$$

where $\bar{x} = x/L$, coordinate axis along the web; $\bar{p} = p/P_a$, air pressure; $\bar{h} = h/\sigma_o$, web-guide clearance. In Eq. (19) the following nondimensional parameters appear as coefficients: $A = 12(\kappa^{1/2}/c)^2(c/L)(\sigma_o/L)^{-3}$, porosity parameter; $B = 6\mu V_x L/P_a \sigma_o^2$, bearing number. The web thickness c , and asperity height σ_o are also scaled with the wrap-length L .

The nondimensional equation for the web displacement can be obtained as:

$$\begin{aligned} S \left(\left(\frac{c}{L} \right)^4 \frac{d^4 \bar{w}}{d\bar{x}^4} + \left(\frac{c}{R} \right)^2 \bar{w} \right) - \left(\frac{c}{L} \right)^2 \left((\bar{N} - V^2) \frac{d^2 \bar{w}}{d\bar{x}^2} - \frac{d\bar{N}}{d\bar{x}} \frac{d\bar{w}}{d\bar{x}} \right) \\ = \left(\frac{c}{R} \right) [C(\bar{p}-1 + \bar{p}_o(1-\bar{h}^2)\mathcal{H}) - \bar{N}] \end{aligned} \quad (20)$$

where $\bar{w} = w/c$, web displacement; $\bar{p}_o = p_o/P_a$, asperity compliance; $\bar{N} = N/T$, in-plane stress resultant. The following nondimensional parameters are obtained as coefficients: $S = [E/P_a(1-\nu^2)](c/R)(P_a R/T)$, stiffness parameter; $V = V_x/(T/\rho_a)^{1/2}$, speed ratio; $C = P_a R/T$, compressibility ratio.

In-plane equilibrium given in Eq. (12) can be nondimensionalized as

$$\frac{d\bar{N}}{d\bar{x}} = -f\beta C \bar{p}_c \quad (21)$$

where $\bar{p}_c = p_c/P_a$, contact pressure. Equations (14) and (18) are nondimensionalized as

$$\left(\frac{\sigma_o}{L} \right) \bar{h} = \left(\frac{c}{L} \right) \bar{w}' + \bar{\delta} \quad (22)$$

$$\bar{w} = \bar{w}' - \bar{w}_{qe} \quad (23)$$

Solution Method

Equations (19)–(23) along with the appropriate boundary conditions describe the mechanics of a porous web moving over a cylindrical guide. By substituting Eq. (23) in (20) four coupled equations are obtained which are solved numerically. A stacked iteration scheme where each equation is solved sequentially is employed. Equations (19) and (20) are nonlinear. They are discretized using standard finite-difference formulation and solved by Newton's method [6]. After discretization and necessary Taylor series expansions, Eqs. (19)–(21) can be represented as

$$\mathbf{K}_p^{(i)} \cdot \Delta \mathbf{p}^{(i+1)} = -\Delta \mathbf{r}_p^{(i+1)} \quad (24a)$$

$$\mathbf{K}_w^{(i)} \cdot \Delta \mathbf{w}^{(i+1)} = -\Delta \mathbf{r}_w^{(i+1)} \quad (24b)$$

$$\mathbf{K}_N \cdot \mathbf{N} = \mathbf{r}_N \quad (24c)$$

where \mathbf{K}_p , \mathbf{K}_w , and \mathbf{K}_N are the tangent stiffness matrices for Eqs. (19)–(21), respectively. The web tension, displacement, and air pressure vectors are \mathbf{N} , $\Delta \mathbf{w}$, and $\Delta \mathbf{p}$. The residuals are given by the vectors \mathbf{r}_N , $\Delta \mathbf{r}_w$, and $\Delta \mathbf{r}_p$. The superscript i is the iteration number. The solution algorithm is composed of two sweeps. In the first step, the air pressure calculations are turned off and the quiescent equilibrium is found by solving Eq. (24b) by itself. This step gives the \mathbf{w}_{qe} vector required for reference state adjustment. In the second sweep, all three equations of (24) are solved simultaneously as described by Müftü and Benson [6].

Results

Parameters Considered. The method outlined in the previous sections is used to predict the tension change for different web handling parameters. The number of independent variables required to describe the problem reduce from fifteen² to nine as a result of the nondimensionalization. Even nine independent, nondimensional parameters are too many to consider in a single article. Here the emphasis is given on studying the effect of the porosity parameter A and the contract pressure parameters \bar{p}_o and σ_o/L on the tension change $\Delta N/T$. The following values of these parameters are used:

$$10^2 \leq A \leq 10^8, \quad \bar{p}_o = 0.1, 1, 10, \quad \sigma_o/L = 2.5, 5, 10 \times 10^{-6}$$

The values of the remaining six nondimensional groups (S , B , V , c/R , c/L , C), and some of the material (E , ν , ρ_{mat} , r) and ambient air properties (P_a , ρ_{air} , μ) are assumed as given in Table 1. Then, it can be shown that while these nondimensional groups and physical properties are constant, a unique relation would exist between ϕ and the nondimensional parameters A and σ_o/L . The Appendix gives the two equations which define this relation. For the values indicated above the A -vs- ϕ variation is given in Fig. 4. Note that by using the values given in Table 1 and the definition of A , the normalized permeability corresponding to each A value can also be calculated: The $\kappa^{1/2}/c$ values, which can be thought as representing the order of magnitude of the nondimensional pore size, are also plotted in this figure. Thus it can be seen that higher fiber volume fraction results in lower permeability, hence smaller A values.

²The coefficient of friction f , the wrap-angle β , and the fiber radius r do not enter the nondimensionalization.

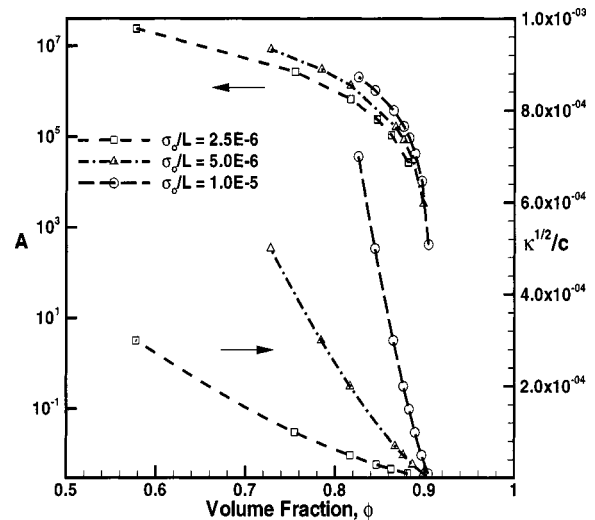


Fig. 4 The porosity parameter A and the normalized permeability $\kappa^{1/2}/c$ as a function of fiber volume fraction ϕ in a web. The different curves for different σ_o/L are calculated while all the problem parameters are kept constant as given in Table 1.

Table 1 The parameter ranges used in the examples. Dimensional values are representative of a paper web used in printing applications. Density of the web material is given by ρ_{mat} .

Non-dimensional		Dimensional	
A	10^2 - 10^8	E (GPa)	6.65
B	300	ν	0.3
S	2009	P_a (kPa)	101.3
V	0.1	r (μm)	4
c/L	3.5×10^{-4}	ρ_{mat} (kg/m^3)	1800
c/R	5.5×10^{-4}	μ (P.a.s)	1.82×10^{-5}
$P_a R/T$	50.7	ρ_{air} (kg/m^3)	1.2
P_o/P_a	0.1, 1, 10		
σ_o/L	$2.5, 5, 10 \times 10^{-6}$		
f	0.23		

Equilibrium Solution. A typical equilibrium solution of the governing equations is presented in Fig. 5 for $A = 1.65 \times 10^5$, $\bar{p}_o = 1$, and $\sigma_o/L = 5 \times 10^{-6}$. In this figure, web-guide clearance \bar{h} , web tension \bar{N} , air pressure \bar{p} , and contact pressure \bar{p}_c are plotted along the web. The wrap region spans the $0 \leq \bar{x} - \bar{x}_C \leq 1$ range and the web motion is in the increasing \bar{x} direction. Figure 5(a) shows that interface has two distinct regions of no-contact and contact followed by an exit region.

The *no-contact* region is located on the entry side of the interface and spans approximately the $0 \leq \bar{x} - \bar{x}_C \leq 0.42$ range. In this region, the belt-wrap pressure is balanced by the pressure of the entrained air which has a superambient value (i.e., $\bar{p} - 1 > 0$). Due to airflow through the web thickness, the pressure drops gradually along the interface until $\bar{x} \approx 0.42$, then it reduces to nearly ambient value at $\bar{x} \approx 0.46$. In the no-contact region, a linear drop of the web-guide clearance is seen from $\bar{h} \approx 5.4$ to the level of asperity engagement, $\bar{h} \approx 1$.

In the *contact* region, which approximately spans the $0.42 \leq \bar{x} - \bar{x}_C \leq 0.98$ range, the web is supported by solid body contact. Figure 5(a) shows that \bar{h} varies in the range 0.84–0.87, indicating that the asperities are compressed approximately 13–16% due to belt-wrap pressure. The figure also shows that the web tension \bar{N} increases linearly from 1 to 1.23 due to sliding friction. This variation of the web tension causes the belt-wrap and contact \bar{p}_c pressures to vary linearly in the sliding direction.

In the *exit* region, shown in detail in Fig. 5(b), the typical sinusoidal pressure variation of the elastohydrodynamic lubrication is seen. The contact pressure provides balance where air pressure becomes subambient. Contact pressure values exceeding N/R can occur in this region.

Figure 5 shows that the calculated tension increase is $\Delta N/T = 0.23$. On the other hand, the belt-wrap formula given in Eq. (1) predicts a higher value, $\Delta N/T = 0.44$. This difference in the two predicted $\Delta N/T$ values is not surprising, as the length of the contact region is less than the length of the entire wrap region. A reasonable question then becomes, if the belt-wrap formula would predict the same value as the numerical procedure if the length of the contact region is used. The contact region is $\sim 0.56L$ long as shown in Fig. 5(a). Using this value in the belt-wrap formula gives $\Delta N/T = 0.22$. The difference between the numerically calculated value (i.e., $\Delta N/T = 0.23$) and the modified tension change from the belt-wrap formula is due to the variations in contact pressure predicted by the numerical solution. The belt-wrap formula does not account for these variations and underestimates the tension change.

Effect of Permeability. The effect of web permeability on web-guide spacing, air pressure, and contact pressure is shown in Figs. 6(a–c), respectively. Figure 6(a) shows that, in the case of the highest fiber volume fraction, $\phi = 0.9$, the web-guide clearance is nearly uniform (i.e., $\bar{h} \approx 5.6$) in the wrap-region. For more

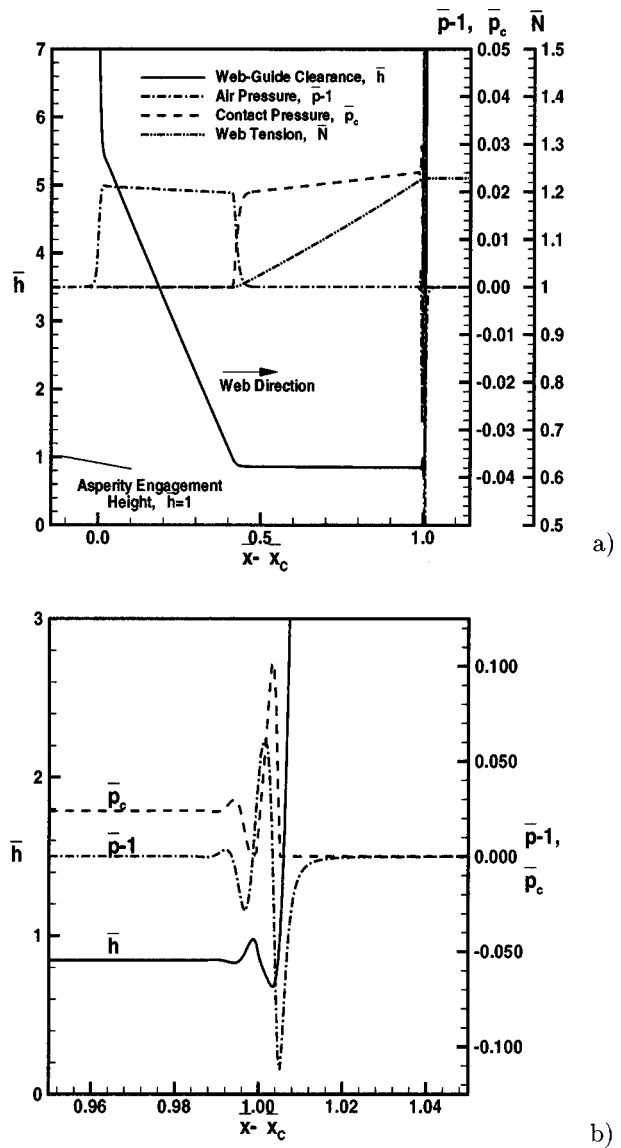


Fig. 5 The steady-state equilibrium conditions in the web-guide interface. Note that the web is in contact near the exit side of the interface ($\phi = 0.88$, $\sigma_o/L = 5 \times 10^{-6}$, $\bar{p}_o = 1$).

permeable webs, the web-guide clearance is no longer uniform, but it linearly decreases starting from the entry region. For example, in the case of $\phi = 0.89$, the web still floats over the guide but its clearance decreases from $\bar{h} = 5.6$ to 3.5 over the wrap-region. For even lower ϕ 's, the slope of the clearance declines even further and contact occurs.

Figure 6(b) shows air pressure profiles. A distinct decrease in the air pressure in the interface, even in the no-contact region, is seen in these profiles. This decrease is due to diffusion of air through the web.

The contact pressure distribution for different volume fractions is presented in Fig. 6(c). As indicated before, in the contact-region, the web equilibrium is provided by the balance between the belt-wrap and contact pressures. A careful investigation of this figure shows that when the web starts to contact the guide, the contact pressure value is approximately equal to T/R . Then further along the contacting interface, \bar{p}_c linearly increases as the web tension increases due to sliding contact.

It should also be noted that the web-guide clearance at the entry $\bar{h}(0)$ is nearly constant for all of the cases considered as shown in

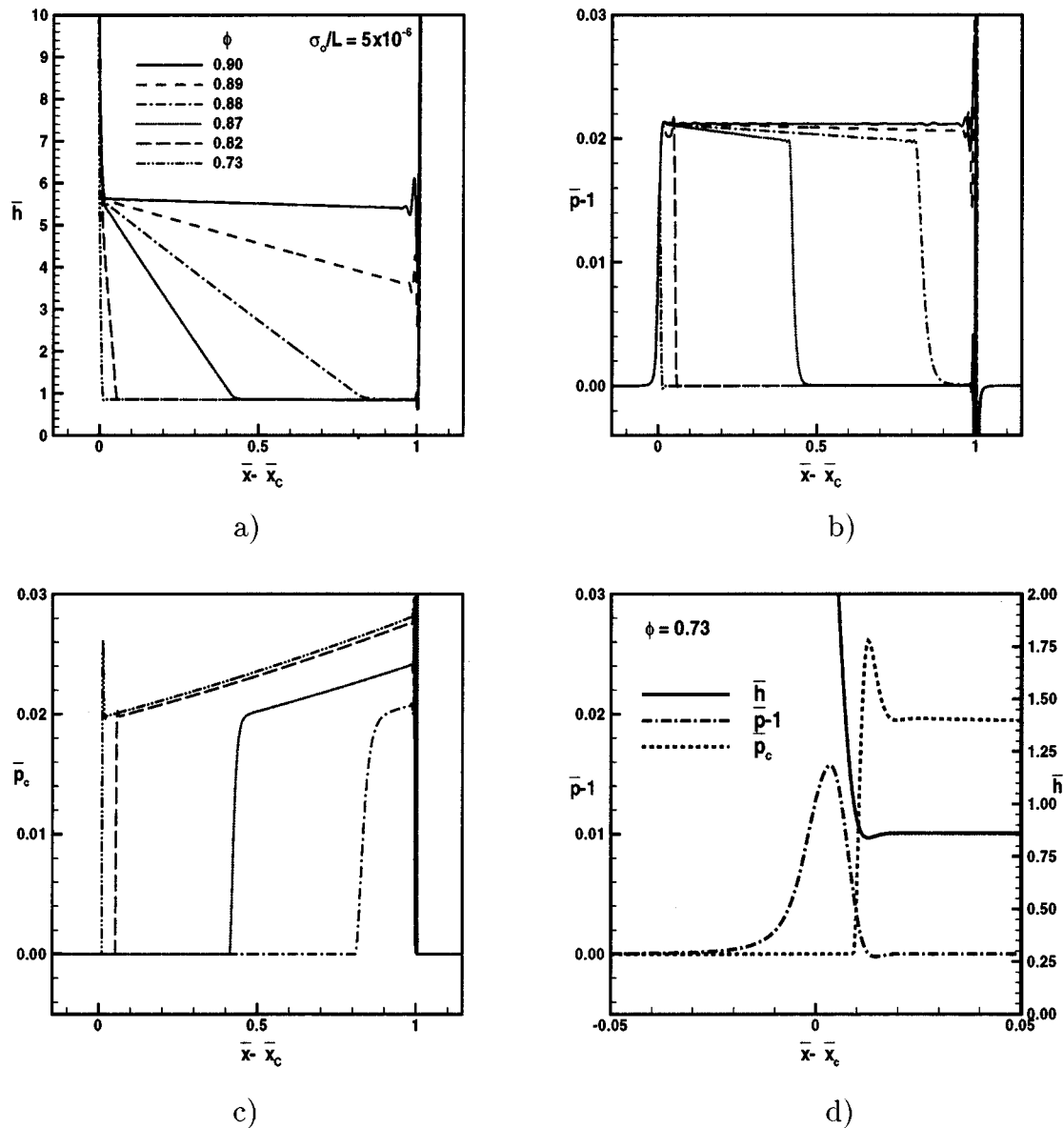


Fig. 6 The web-guide clearance \bar{h} , air pressure \bar{p} , and contact pressure \bar{p}_c variation for different values of fiber volume fraction ϕ values are given in plots (a–c) for $\sigma_o/L=5 \times 10^{-6}$, $\bar{p}_o=1$. Plot (d) gives the detail of the entry region for $\phi=0.73$.

Fig. 6(a). This indicates that on the entry side air entrainment is not significantly affected by diffusion through the web.

A boundary effect can be seen near the entry region of the interface for $\phi=0.73$ and to a lesser extent for $\phi=0.82$. Figure 6(d) shows the detail of the area near the entry region for $\phi=0.73$ case. The web reacts to the small air pressure in the entry region, $\bar{x}-\bar{x}_c \leq 0$, with a relatively large displacement because the belt-wrap pressure is relatively small in this region. As this is a relatively permeable web, the air pressure does not fully develop to provide support for the web in the wrap region, $\bar{x}-\bar{x}_c \geq 0$, and the web contacts the guide near $\bar{x}-\bar{x}_c \approx 0.01$. The coupled system compensates for the lack of contact pressure in $0 \leq \bar{x}-\bar{x}_c \leq 0.01$ by a localized increase in contact pressure between $0.01 \leq \bar{x}-\bar{x}_c \leq 0.018$. This boundary effect is not seen for the higher volume fraction values where the air pressure can rise to levels sufficient to support the web.

Effect of Permeability and Contact Parameters on Traction. The previous sections suggest that the tension in-

crease along the guide is inversely related to the web permeability. It is also reasonable to assume that the contact parameters \bar{p}_o and σ_o/L would affect the tension increase, since the tangential shear in the web is directly proportional to contact pressure. The effect of σ_o/L and ϕ on the tension increase is plotted in Fig. 7, which shows that high fiber volume fraction (low permeability) causes susceptibility to flying (i.e., $\Delta N/T \rightarrow 0$ as $\phi \rightarrow 1$). On the other hand, webs that have low volume fraction of fibers (high permeability) contact the guide (i.e., $\Delta N/T \rightarrow (e^{f\beta} - 1)$ as $\phi \rightarrow 0$). In between the two extreme volume fractions lies a transition range. This figure also shows that for a given ϕ , the smaller σ_o/L values cause less tension increase.

Plotting the tension increase as a function of the fiber volume fraction, as in Fig. 7, indicates that the transition from $\Delta N/T = 0$ to $\Delta N/T \rightarrow (e^{f\beta} - 1)$ occurs at different ϕ ranges for different σ_o/L values. On the other hand, when $\Delta N/T$ is plotted with respect to A , as in Fig. 8, it is seen that the effect of engagement height is nearly reduced to one single curve. The transition from

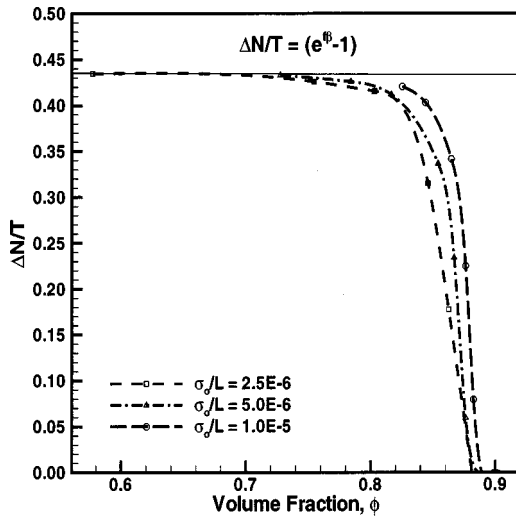


Fig. 7 The effect of nondimensional asperity height on the tension drop $\Delta N/T$ as a function of fiber volume fraction ϕ , for $\bar{p}_o=1$

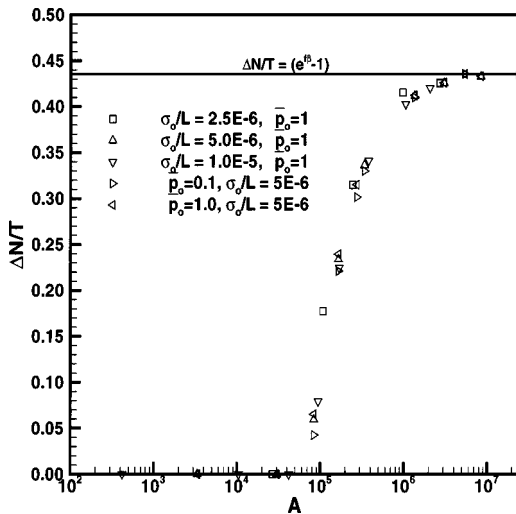


Fig. 8 The effect of asperity engagement height and compliance on the tension drop $\Delta N/T$ as a function of the porosity parameter A

maximum possible traction to complete tension loss is seen to occur in the range $10^5 \leq A \leq 4 \times 10^6$. The effect of changing the asperity compliance parameter is also plotted on the same figure. For $\bar{p}_o = 0.1, 1, \text{ and } 10$ while $\sigma_o/L = 5 \times 10^{-6}$, the asperity compliance parameter also has a small effect in the transition from complete tension loss to maximum possible traction. Therefore it is concluded that for the parameter range studied, the traction loss scales with A and is independent of the contact parameters.

Summary and Conclusions

A steady-state model for analyzing the mechanics of a porous web, moving over a cylindrical rigid guide, is presented. Web porosity is expressed as a function of the fiber volume fraction of the web. A modified Reynolds equation is derived for a bearing with a moving porous surface using Darcy's law and equations of conservation of momentum and mass for air. The web is modeled as a moving cylindrically curved beam. The solid-body contact between the web and the guide is modeled using an empirical

based asperity compliance function. In-plane stress resultant redistribution due to sliding contact is calculated by considering the in-plane stress equilibrium.

The effects of web porosity parameter A and the contact pressure parameters \bar{p}_o and σ_o/L on the tension change are investigated. The relation between the fiber volume fraction ϕ and web permeability $\kappa^{1/2}/c$, for the nondimensional parameter range considered, shows that higher ϕ values result in lower permeability, as expected. It is found that depending on the level of permeability, airflow through the web thickness causes reduction in the pressure of air entrained in the interface. For the parameters considered in this paper, full web-guide separation is achieved only in very high fiber volume fraction cases ($\phi \geq 0.89$). Solid-body contact and sliding causes increase in web tension in the running direction. It is found that the change in web tension scales with the porosity parameter A and is nearly independent of the contact parameters \bar{p}_o and σ_o/L . The transition from full web-guide contact to full separation occurs in the range $10^5 \leq A \leq 4 \times 10^6$.

Acknowledgments

Parts of this work, for the first author, were supported by the National Science Foundation through grant ECS 9615027. The authors would like to thank Dr. Kevin A. Cole of Eastman Kodak Company for his valuable comments.

Appendix

Let the right-hand side of Eq. (3) be denoted by $f(\phi)$. Then, if the physical parameters ($E, \nu, \rho_{\text{mat}}, r$) and ($P_a, \rho_{\text{air}}, \mu$) are assumed to be known, the following relations between the nondimensional and these known dimensional variables can be obtained:

$$f(\phi) = \frac{3E\mu^2 A V^2 (c/L)}{r^2 P_a (1-\nu^2) S B^2 (\sigma_o/L) [\phi \rho_{\text{mat}} + (1-\phi) \rho_{\text{air}}]}, \quad (25a)$$

$$c^2 = \frac{12r^2 (c/L) f(\phi)}{A (\sigma_o/L)^3}. \quad (25b)$$

References

- [1] Daly, D. A., 1965, "Factors Controlling Traction Between Webs and Their Carrying Rolls," *Tappi J.*, **48**, No. 9, pp. 88A–90A, Sept.
- [2] Ducotey, K. S., and Good, J. K., 1998, "The Effect of Web Permeability and Side Leakage on the Air Film Height Between a Roller and Web," *ASME J. Tribol.*, **120**, pp. 559–565.
- [3] Gross, W. A., 1980, *Fluid Film Lubrication*, Wiley, New York.
- [4] Hashimoto, H., 1995, "Theoretical Analysis of Externally Pressurized Porous Foil Bearings-Part 1: In Case of Smooth Surface Porous Shaft," *ASME J. Tribol.*, **117**, No. 1, pp. 93–102.
- [5] Hashimoto, H., 1997, "Effects of Foil Bending Rigidity on Spacing Height Characteristics of Hydrostatic Porous Foil Bearing for Web Handling Processes," *ASME J. Tribol.*, **119**, No. 1, pp. 422–427.
- [6] Müftü, S., and Benson, R. C., 1995, "Modelling the Transport of Paper Webs Including the Paper Permeability Effects," *Advances in Information Storage and Processing Systems-1995*, ASME International Mech. Eng. Congress and Exposition, San Francisco, CA, ISPS-Vol. 1, pp. 247–258.
- [7] Wang, X., 1997, "Finite Element Analysis of Air-Sheet Interactions and Flutter Suppression Devices," *J. Comput. Structures* **64**, No. 5/6, pp. 983–994.
- [8] Ducotey, K. S., and Good, J. K., 1995, "The Importance of Traction in Web Handling," *ASME J. Tribol.*, **117**, pp. 679–684.
- [9] Johnson, K. L., 1985, *Contact Mechanics*, Cambridge University Press, England.
- [10] Patir, N., and Chang, H. S., 1979, "Application of Average Flow Model to Lubrication Between Rough Sliding Surfaces," *ASME J. Lubr. Technol.*, **101**, pp. 220–230.
- [11] Gutowski, T. G., Morigaki, T., and Cai, Z., 1987, "The Consolidation of Laminate Composites," *J. Compos. Mater.*, **21**, pp. 172–188.
- [12] Dave, R., Kardos, J. L., and Dudukovic, M. P., 1987, "A Model for Resin Flow During Composite Processing. Part 2: Numerical Analysis for Unidirectional Graphite/Epoxy Laminates," *Polym. Compos.*, **8**, No. 2, pp. 123–132.
- [13] Lam, R. C., and Kardos, J. L., 1989, "The Permeability and Compressibility and Aligned and Cross-Plied Carbon Fiber Beds During Processing of Composites," *ANTEC '98, SPE*, pp. 1408–1412.
- [14] Bruschke, M. V., and Advani, S. G., 1993, "Flow of Generalized Newtonian

- Fluids Across a Periodic Array of Cylinders," *J. Rheol.* **37**, No. 3, pp. 479–498.
- [15] Bear, J., 1972, *Dynamics of Fluids in Porous Media*, Dover, New York.
- [16] Tichy, J. A., 1994, "A Porous Media Model for Thin Film Lubrication," *ASME J. Tribol.*, 94-Trib-3.
- [17] Bujurke, N. M., Patil, H. P., and Bhavi, S. G., 1990, "Porous Slider Bearing with Couple Stress Fluid," *Acta Mech.*, **85**, pp. 99–113.
- [18] Müftü, S., and Cole, K. A., 1999, "The Fluid/Structure Interaction in Supporting a Thin Flexible Cylindrical Web with an Air Cushion," *J. Fluids Structures*, **13**, No. 6, pp. 681–708.
- [19] Müftü, S., and Benson, R. C., 1996, "A Study of the Cross-Width Variations in the Two Dimensional Foil Bearing Problem," *ASME J. Tribol.*, **118**, pp. 407–414.
- [20] Rabinowicz, E., 1995, *Friction and Wear of Materials*, Wiley, New York.
- [21] Wu, Y., and Talke, F., 1996, "The Effect of Surface Roughness on the Head-tape Interface," *ASME J. Tribol.*, **118**, No. 2, pp. 376–381.
- [22] Greenwood, J. A., and Williamson, J. B. P., 1966, "Contact of Nominally Flat Surfaces," *Proc. R. Soc. London, Ser. A*, **295**, 300–319.
- [23] Rice, B. S., Cole, K. A., and Müftü, S., 1999, "An Experimental and Theoretical Study of Web Traction Over a Nonvented Roller," *Proceedings of the Fifth Int. Web Handling Conference*, Oklahoma State University, Stillwater, OK, June.